Soft Matter

Fractographic Mirror Law for Brittle Fracture of Nonlinear Elastic Soft Materials

Journal:	*Soft Matter*
Manuscript ID	SM-ART-07-2023-000879.R1
Article Type:	Paper
Date Submitted by the Author:	12-Sep-2023
Complete List of Authors:	Kiyama, Ryuji; Hokkaido University, Department of Advanced Transdisciplinary Sciences, Faculty of Advanced Life Science Zheng, Yong; Hokkaido University Nonoyama, Takayuki; Hokkaido University, Department of Advanced Transdisciplinary Sciences, Faculty of Advanced Life Science Gong, Jian Ping; Hokkaido University,

ARTICLE

Fractographic Mirror Law for Brittle Fracture of Nonlinear Elastic Soft Materials

Received 00th January 20xx,
Accepted 00th January 20xx

DOI: 10.1039/x0xx00000x

Ryuji Kiyama[a,b], Yong Zheng[c], Takayuki Nonoyama[a], Jian Ping Gong[a,c]*

Mirror radius analysis of fractured surfaces is a powerful fractographic method for determining the cause of failure in linear elastic hard materials because it does not require prior loading information. However, mirror analysis for soft materials is lacking. In this study, we established a general mirror radius law for nonlinear elastic soft materials using highly deformable brittle hydrogels. The fracture stress and mirror radius follow a -1 power law, which differs from the -0.5 power law for linear elastic hard materials. The constant in the power law is related to the fracture energy of the material. This discovery provides insights into fracture mechanisms and leads the way for applying fractography to soft materials.

Introduction

Soft materials such as rubbers and hydrogels are widely used for various applications, including soft robotics, stretchable electronics, and tissue engineering(*1–6*). In particular, robust and tough hydrogels invented in the last 20 years are promising materials for stretchable load-bearing biomaterials due to their excellent biocompatibility and mechanical compatibility with living tissues(*7–10*). The load limit of a material is an indispensable parameter for practical use, and many scientists have studied its fracture. The fracture mechanism of hard materials such as ceramics and glasses is well understood by linear elastic fracture mechanics (LEFM), enabling precise prediction of the fracture condition of any complex geometry based on the critical stress intensity factor, K_{IC} (N/m$^{3/2}$) (material-specific toughness index), and stress distribution calculated using finite element methods. However, the fracture mechanism of soft materials is not well understood because they are highly deformable, nonlinear elastic, and dissipative(*11–14*). Moreover, LEFM could not be applied to these materials. Recently, many studies have been conducted to estimate the realistic fracture behavior of this class of materials. For example, instead of material fracture toughness K_{IC} of LEFM, many studies applied other useful toughness indexes such as *J*-integral and crack-tip opening displacement to investigate the fracture of soft materials(*15–18*).

[a] *Faculty of Advanced Life Science, Hokkaido University, N21W11, Kita-ku, Sapporo 01-0021, Japan.*
[b] *Creative Research Institution (CRIS), Hokkaido University, N21W10, Kita-ku, Sapporo 001-0021, Japan.*
[c] *Institute for Chemical Reaction Design and Discovery (WPI-ICReDD), Hokkaido University, N21W10, Kita-ku, Sapporo 001-0021, Japan.*
Electronic Supplementary Information (ESI) available: [details of any supplementary information available should be included here]. See DOI: 10.1039/x0xx00000x

Analysis of the fracture surface morphology of a material, known as fractography, is a powerful method for determining the fracture cause because it does not require prior information on how the sample is loaded(*19–22*). **Fig. 1** shows the typical brittle fracture process of a material. Under tensile deformation, cracks begin to progress from the initial defect and pass through the material while being accelerated by the stored strain energy. When the crack reaches the upper limit velocity, which is comparable to the sonic speed of the material, multiple crack surfaces (crack branching) are generated to compensate for the excess strain energy instead of crack acceleration; Therefore, the fracture surface exhibits a characteristic geometry with a smooth circular face (mirror surface) centered on the starting point of the fracture and a radially rough face (mist-hackle surface) outside the smooth circle. The radius of a smooth circle is called "mirror radius *r* (m)," considered as a parameter related to fracture mechanics(*20–22*). For linear elastic hard materials such as glass, the mirror radius is correlated to the fracture stress σ_F (N/m^2) using a semi-empirical formula(*19*, *23*, *24*):

$$\sigma_F = A_L \cdot r^{-0.5} \quad (1)$$

where the mirror constant A_L (N/m$^{3/2}$) is a characteristic material constant. Here, we denote the mirror constant as A_L for linear elastic materials to distinguish it from that of non-linear elastic materials, A_{NL}. Some studies have indicated that A_L is a parameter related to the stress distribution around the crack tip and is proportional to K_{IC}. Thus, K_{IC} can be estimated from mirror radius observation(*19*, *23*).

What is the corresponding mirror radius law for nonlinear elastic soft materials? They have a different crack tip stress field from linear elastic materials, so they should fracture different way. In this study, we intend to establish a fractographic law for the brittle fracture of soft materials.

We adopted chemically crosslinked hydrogels as model materials, which are ideal nonlinear elastic soft materials without strain-rate-dependent deformation. However, common chemical hydrogels are too weak to observe the hackle regions because their mirror radii are larger than the experimentally available sample size. In this study, we overcome this problem by adopting the Double Network concept to synthesize hydrogels (DN gels) with the proper strength for fracture mirror analysis. DN gels consist of two elastic networks in contrasting structures: a short-chain network that breaks sacrificially upon stretching and a long-chain network that maintains the elasticity of the hydrogel(*7*). DN gels exhibit much higher fracture strengths and toughnesses than the simple sum of the two constitutive networks. Since the deformation of DN gels is velocity-independent of rubber elasticity, they are excellent model materials for studying the nonlinear elastic fracture of soft materials(*16*).

In this study, we identified a semicircular mirror region and a mist-hackle region on the fracture surfaces of DN hydrogels with various compositions. We also found a new semi-empirical power law with a slope of -1 between the fracture stress and mirror radius for nonlinear elastic soft materials. Interestingly, in this equation, the material constant A_{NL} (N/m= J/m^2) has a dimension of *J*-integral, indicating that it is related to the fracture toughness of the material. This is consistent with the material constant A_L of linear elastic hard materials, which is related to the critical stress intensity factor, K_{IC}.

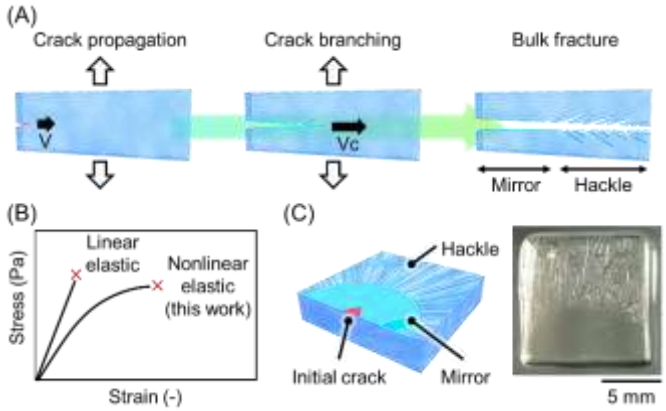

Fig. 1 Brittle fracture process. (A) Schematic illustration of crack propagation process in a brittle material under uniaxial tensile deformation. (B) Stress-strain curves of typical linear elastic material and nonlinear elastic material. (C) Schematic brittle fracture surface (left) and optical image of the fractured surface of a tough DN hydrogel (8/4) experienced a tensile deformation (right). This DN gel showed a typical brittle fracture surface.

Materials and Methods

1 Materials

2-Acrylamido-2-methyl propanesulfonic acid (AMPS: monomer) was provided by Toagosei Co., Ltd., Japan. Dimethylacrylamide (DMAAm: monomer), *N, N'*-methylenebisacrylamide (MBAA: crosslinker), 2-oxoglutaric acid (α-keto: initiator), and iron (III) chloride hexahydrate were purchased from Wako Pure Chemical Industries Ltd., Japan. All chemicals were used as received.

2 Gel synthesis

The PAMPS/PDMAAm DN gel was synthesized according to a previously reported protocol [7]. First, PAMPS gel was synthesized via UV radical polymerization in a mold made from a silicone spacer sandwiched between two glass plates. The UV irradiation time was 8 h, and the mold was deoxidized overnight in an argon chamber. The precursor solution comprised 1 mol/L AMPS as the monomer, 2–8 mol% MBAA as the cross-linker, and 0.1 mol% α-keto as the initiator. mol% indicates the ratio to the monomer concentration. Then the synthesized PAMPS gel was removed from the mold and soaked into the PDMAAm network precursor solution containing 1–4 mol/L DMAAm, 0.1 mol% MBAA, and 0.1 mol% α-keto until equilibrium for one day. We code the gels as (1st crosslinker mol%: C_1)/(2nd monomer mol/L: M_2), similar to the DN gel (8/2). The PAMPS gel containing the PDMAAm network precursor solution was sandwiched between two glass plates and irradiated with UV for a 2nd polymerization for 6 h in an Ar atmosphere. After polymerization, the obtained DN gels were immediately used for experiments without water absorption. The thickness of the DN gels was adjusted to approximately 1 cm by adjusting the thickness of the silicone spacer of the PAMPS mold. PAMPS and PDMAAm single-network gels were also synthesized by UV initiated radical polymerization in glass molds. The precursor solution composition of PAMPS gel was 1 mol/L AMPS, 4 mol% MBAA, and 0.1 mol% α-keto, and that of PDMAAm gel was 4 mol/L DMAAm, 0.1 mol% MBAA, and 0.1 mol% α-keto. PAMPS and PDMAAm gels were used in the experiment in water-swollen and non-swollen states, respectively. Depending on the composition of the two networks, DN hydrogels can be tuned from brittle to ductile, which could provide a suitable material window for studying the fractographic law of nonlinear elastic materials.

3 Tensile test

The tensile mechanical properties of the DN gels were examined using a mechanical tester (Tensilon RTC-1310A; Orientec Co., Japan). The samples were cut into dumbbell shapes (JIS K 6251, Type 2:2 cm gauge length and 1 cm width) using a programmed laser cutter (ULR-60, Universal Laser Systems, US). Then, we introduced a triangular initial crack in the middle of the gauge by using a fine microtome knife with an edge thickness of 76 μm. A tensile test was performed at a 100 mm/min speed, during which the sample deformation was recorded by video. After the tensile fracture, we immediately observed the fractured surface using optical microscopy (SZX-12, Olympus, Japan) and determined the mirror radius by measuring the distance from the initial crack to the hackle region. The

transition from mirror region to hackle region varies with the resolution of the measuring equipment because the roughness gradually increases between the two regions. Since we used an optical microscope in this study, the hackle region was defined as a surface on which the structure was larger than the wavelength of visible light (400–800 nm). Each test was performed on more than ten samples.

Because of the large deformation of the DN gels, we could not use the nominal strain and nominal stress to understand the fracture process in the deformed state. The true fracture stress and true mirror radius in the deformed state during crack propagation were calculated as follows: Because gels are incompressible materials at our observation time scale, the stretch ratio in the lateral direction is $1/\sqrt{\lambda}$ for a stretch ratio λ in the tensile direction. We measured the sample widths in the undeformed and deformed states immediately before the fracture in the video and then calculated the fracture stretch ratio λ_F from the lateral deformation ratio. Finally, we calculated the true fracture stress: $\sigma_F = \sigma_F(Nominal)\lambda_F$ and the true mirror radius: $r = \frac{r_0}{\sqrt{\lambda_F}}$ at sample fracture, where r_0 is mirror radius of the samples at undeformed state.

Note that in the dumbbell-shaped specimens without inserted cracks, fracture tend to occur near the handle of jig, and in such cases, the fracture surface is often not flat reflecting stress distribution near the jig, making it unclear how to define the mirror radius. Thus, in this study, we introduced initial crack at the surface of sample gauge side to ensure that the crack propagates straight. Sometimes, we can get other type of fracture. We put an example of the gel broken from internal defect in **Supporting Fig. 1** (contaminant probably introduced during gel preparation). We can see obvious formation of mirror radius also in such natural fracture case.

4 Roughness observation by 3D laser microscope

To observe the macroscopic surface morphology of the fractured DN hydrogels, 3D laser microscopy (VK-9710; KEYENCE, Japan) was performed. The wavelength of the laser source was 408 nm. A line-scanning image of the fractured surface was obtained, and a roughness scan was performed by taking a simple moving average of nine data points from the raw data.

5 Roughness observation by transmission electron microscopy (TEM)

TEM (H-7650, Hitachi, Japan) was used to observe the microscopic surface morphology of the fractured samples. Staining was performed as described in our previous study [28]. Briefly, the DN gel was immersed in a staining solution of 2.5 M $FeCl_3$ for one day at room temperature, after which the gels were immersed in pure water to increase the pH, and amorphous ferric oxide nanoparticles were mineralized on the PAMPS network, especially near the bulk surface. To prepare the specimen for TEM observation, the hydrogel was frozen in liquid nitrogen, and the water in the hydrogel was exchanged with ethanol and acrylic resin (London Resin white, medium) in the chamber of an automatic freeze substitution system (EM AFS2, Leica Microsystems, Germany). The final change in the thickness of the resin-cured specimen was within 10% of that of the DN gel in water. Then, 100-nm thick sections of the resin-cured specimens were cut using an ultra-microtome (EM UC7i, Leica Microsystems, Germany) and placed on a carbon-supported copper mesh grid. Transmission electron microscopy (TEM) observations were performed at an electron gun acceleration voltage of 100 kV.

6 Critical energy release rate measured by pure shear test

The fracture energy, which is defined as the energy required to create a new unit surface, is characterized by the critical energy release rate G_c. Pure shear tests were performed to determine G_c according to a previous report [27]. First, 1 mm-thick gel samples were cut into rectangular shapes of 50 mm width and 30 mm height using a programmed laser cutter. The samples were clamped using a jig at an initial height of 10 mm (l_0), and a 10 mm initial crack was inserted at the middle of the side using scissors. The samples were stretched at a tensile velocity of 100 mm/min until they fractured. The strain ε_c at the onset of crack propagation was determined. Next, the cyclic stress-strain curves of the unnotched samples with the same geometries as the notched samples were obtained for the preset strain ε_c, and the energy release rate of the samples G_c was calculated using the following equation: $G_c = W_{el}(\varepsilon_c) \times l_0$. Here $W_{el}(\varepsilon_c)$ is the stored energy density of the sample stretched to the critical strain ε_c calculated from the unloading stress-strain curves.

7 Statistical analysis

Each test was performed on more than ten samples. All samples with the same composition showed good mechanical reproducibility. Samples were excluded if the fracture started from inevitable scratches on sample surface or the mirror radius: r_0 exceeded sample size. All data are presented as means ± standard error of the mean.

Results and discussion

Mirror radius formation by crack branching

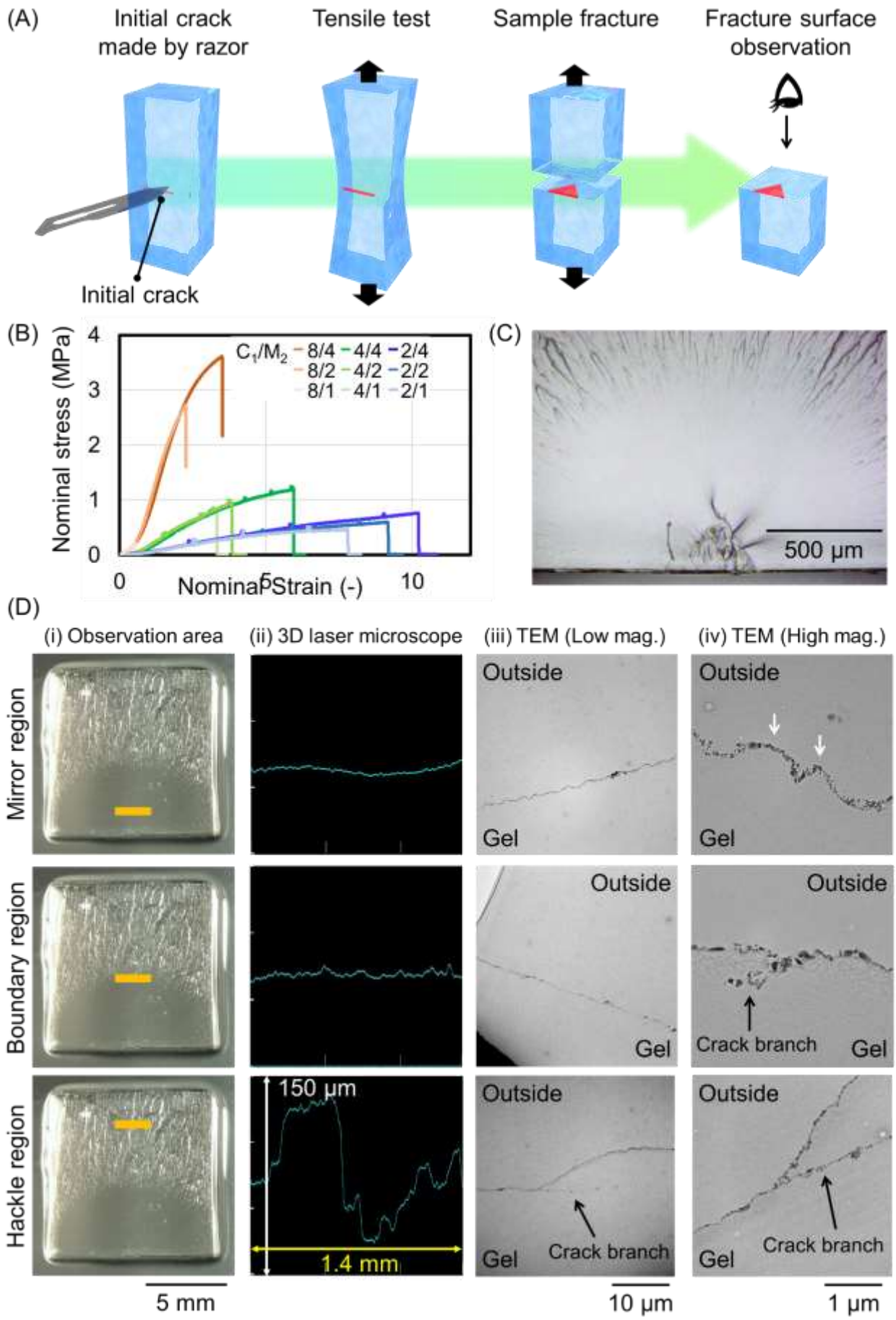

Fig. 2 Fracture surface analysis of tough DN gels. (A) Schematic diagram of the experimental method. (B) Tensile stress-strain curves of un-notched PAMPS/PDMAAm DN gels prepared with various compositions. (C) Optical image of a fractured surface of DN gel (8/2). The triangle-shaped initial crack, mirror region, and mist-hackle region are clearly visible. (D) Macro- and micro-roughness features of a fractured surface of DN gel (8/4). Yellow lines in the photographs of column (i) represent the observation area of 3D laser images in column (ii) and TEM images in columns (iii, iv). White and black arrows in the TEM images indicate surface roughness and branched crack, respectively.

First, we synthesized tough DN hydrogels consisting of poly(2-acrylamido-2-methyl propanesulfonic acid) (PAMPS) as the brittle first network and poly(N,N-dimethylacrylamide) (PDMAAm) as the stretchable second network following the previous report(*7*). In this study, we focused on brittle fractures. Therefore, we prepared DN gels without yielding or necking. To obtain DN gels of varied mechanical properties, we tuned the cross-linker density C_1 (mol%) of the 1st network and the monomer concentration of the 2nd network M_2 (M), while the monomer concentrations of 1st network, the cross-linker density of the 2nd network, and density of initiators of the two networks were fixed to 1 M, 0.1 mol%, and 0.1 mol%, respectively. Here mol% are respective to the corresponding monomer concentration in the network. The Young's modulus of the DN gels increased with C_1, whereas the fracture strain increased with M_2. The sample is denoted as (C_1/M_2). The sample was cut into a dumbbell shape with a central cross-sectional area of 1 cm × 1 cm, and a triangle-shaped initial crack perpendicular to the tensile direction was introduced using a sharp knife. Tensile testing was performed at 100 mm/min until the sample fractured. The experimental details are described in **Fig 2A** and Materials and Methods section. The stress-strain curves and a representative movie of the tensile test are shown in **Fig. 2B** and the **Supplementary video**. The mechanical behavior of the DN gels varied with chemical composition. Typical DN gels show complex deformation accompanied by necking, in which a portion of the gel specimen becomes slender, corresponding to yielding behavior(*8*). However, by tuning gel composition, all the samples used in this study exhibited typical nonlinear elastic S-shaped stress-strain curves without yielding. The gels were significantly deformed in all compositions without crack growth before the fracture. When the crack began to grow, global fracture immediately occurred in a brittle manner. As shown in **Fig 2B**, Young's modulus and fracture strains of the DN gels were tuned separately by changing the cross-linker density of the 1st network C_1 and the concentration of the 2nd network M_2.

The mirror radius r on the fracture surface was immediately measured using an optical microscope after the fracture (**Fig. 2C**). A smooth semicircular mirror region was formed centered on the initial crack, and a mist-hackle region with radial bumps was formed on the outer circumference. Occasionally, some materials have another drastic roughness transition inside the mist-hackle region. Therefore, in that case, mist regions with relatively small unevenness and hackle regions with relatively large unevenness are discussed separately. However, there is no clear roughness transition for other materials including our tough gels, and it is difficult to define mist and hackle boundaries(*19*).

To confirm that the mist hackle pattern on the fractured surface corresponded to crack branching, we observed the microscopic structure of the surface using a 3D laser microscope and transmission electron microscope (TEM) (**Fig. 2D**). The mirror region near the initial crack was flat at the macroscale. However, a small surface roughness at the micrometer scale (white arrow in the TEM image) was observed in TEM images. This roughness is probably due to the network heterogeneity of the gel(*25*) or crack tilting caused by the stress field in front of a fast crack that has maximum stress in the out-of-plane direction(*26*). The boundary region was also almost flat at the macroscale, but shallow crack branching (black arrow in the TEM image) began to form at the microscale. In the mist-hackle region, multiple crack branching leads to huge roughness at the macroscale, and deep crack branching from the main crack plane (black arrow in the TEM image) is observed at the microscale. From the above results, we confirmed that brittle fractures with crack branching occurred during the fracture of the soft hydrogels, forming mirror and mist-hackle regions on the fracture surface.

Additionally, we observed the fracture surfaces of other hydrogels that were brittle but not tough (**Supporting Fig. 2**). The samples were a single-network (SN) PAMPS gel and SN PDMAAm gel, which are the constituent materials of tough DN gels. However, only a smooth mirror region was observed in both samples, and no mist-hackle region was observed on the fracture surface. We can speculate that the mirror radius exceeded the sample cross-section (1 cm × 1 cm) because the mirror radius is inversely proportional to the fracture stress. These SN gels had relatively small true fracture stress (10–100 kPa) compared to the DN gels (200–10000 kPa). Significantly larger samples were required to apply mirror radius analysis to weak gels, which is technically difficult.

Relationship between mirror radius and fracture stress

The relationship between the mirror radius and fracture stress was evaluated based on the tensile fracture test. **Fig. 3** shows the double logarithmic plot of the true fracture stress (σ_F) against the true mirror radius (r) of a DN gel (8/2). The fracture stress was tuned by varying the depths of the initial cracks. In the analysis, we removed data for low σ_F samples that show the mirror surface too close to the sample edge. In **Fig. 3**, similar to linear elastic materials, the gels with higher σ_F show smaller mirror radii, and gels with lower σ_F show larger mirror radii. This relationship was well-approximated by a negative power law with a slope of approximately -1.2.

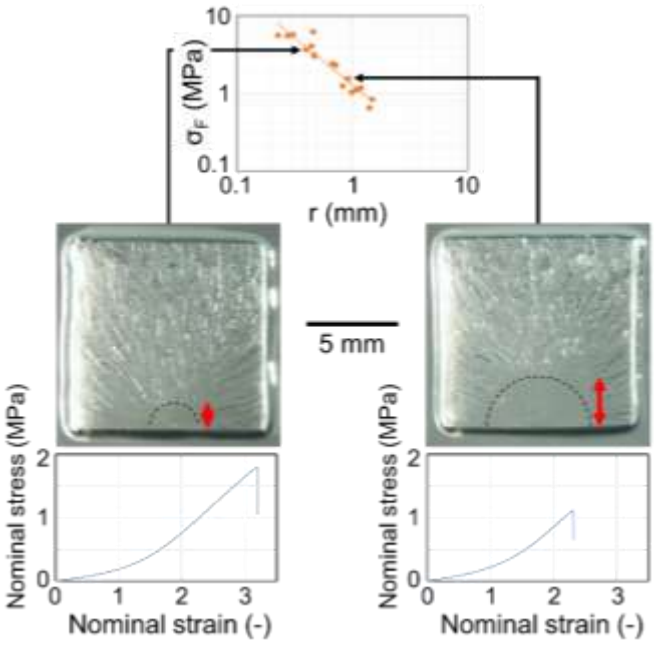

Fig. 3 Relationship between true fracture stress (σ_F) and true mirror radius (r) for DN gel (8/2). Fracture surface images and nominal stress-strain curves of two representative samples with small and large fracture stress are shown. Red arrows in the images indicate a nominal mirror radius at an undeformed state.

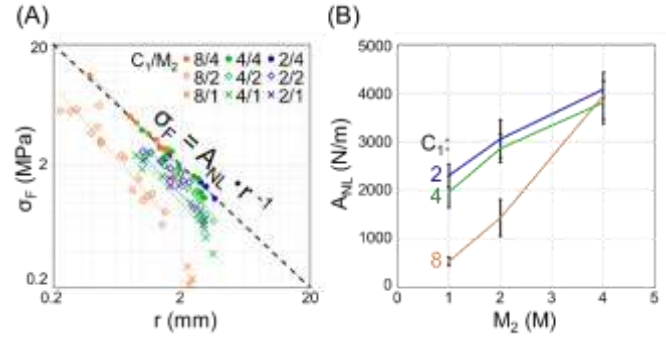

Fig. 4 Universal relationship between true fracture stress (σ_F) and true mirror radius (r) for nonlinear elastic DN gels. (A) σ_F versus r of DN gels with various compositions. The black dashed line in the graph indicates the slope of -1. (B) Material constant A_{NL} for DN gels with various compositions.

To investigate the universality of the power-law correlation, fracture surface analysis of DN gels with various compositions was conducted (**Fig. 4A**). The measurement range of the mirror radius differs depending on the sample because the crack sensitivity of the sample determines the lower r limit. For samples with high crack sensitivity, uncontrollable fracture occurs not from the initial crack inserted on the sample side face but from minor scratches inevitably created during sample preparation. Therefore, some samples (especially 8/1) had a narrow measurement range. However, this did not affect the analytical results. In **Fig. 4A**, all tough gels showed power law exponent in the range of -0.95 to -1.25, which could be fitted by the following equation,

$$\boldsymbol{\sigma_F = A_{NL} \cdot r^{-1}} \quad (2)$$

where A_{NL} (N/m) is a constant with dimensions similar to those of the J-integral, J (N/m). In nonlinear elastic materials, J plays a similar role as the stress intensity factor for a linear elastic material(*12*). Using the above equation, we calculated A_{NL} for each composition of soft DN gels, as shown in **Fig. 4B**. The range of A_{NL} is 500–4000 N/m. The A_{NL} increased as the monomer concentration of the second network M_2 increased, whereas the cross-linker density of the first network C_1 had little effect, except in two samples (8/1 and 8/2). To confirm that the A_{NL} is a material-specific value independent of the experimental conditions, we evaluated A_{NL} with different sample shapes and tensile velocities of the DN gel (8/2) (**Supporting Fig. 3**). Regardless of the sample size and tensile speed, A_{NL} was almost constant at 1500 N/m, indicating that A_{NL} is a material constant that depends only on the gel composition.

Considering the similarity between equations (2) and (1) for linear elastic hard materials, we expected that A_{NL} would also correlate with the material toughness index. Thus, we compared A_{NL} with the toughness of the gels. The critical energy release rate at crack initiation (G_c) of the DN gels (4/M_2) was measured using a pure shear test(*27*). G_c increased slightly with M_2, showing the same trend as A_{NL}. However, the values of G_c were in the range of 500–1000 N/m, which were lower than A_{NL} (2000–4000 N/m) (**Supporting Fig. 4**). This is reasonable because A_{NL} is related to the energy release rate during crack propagation whereas G_c is the energy release rate at crack initiation.

Finally, we compared mirror radius equations (1) and (2) with the stress field around the crack tip. LEFM predicts that the stress field around crack tips follows a universal singularity of the form $\boldsymbol{\sigma \sim x^{-1/2}}$ while non-LEFM predicts a form $\boldsymbol{\sigma \sim x^{-1}}$ (*12*, *18*), here $\boldsymbol{x}$ (m) is distance from crack tip. The universal mirror radius laws observed for the linear and nonlinear elastic materials have similar forms with their respective stress fields around the crack tips. This suggests that the stress field around the crack tip governs the fractographic behavior.

Conclusions

We found that the true fracture stress scales with the mirror radius r by a power law of -1 for nonlinear elastic hydrogels. This new semi-empirical formula differs from that of a linear elastic material, which has a power law of -0.5. These two power-law relationships are similar to their respective stress fields around the crack tips, suggesting that the stress field around the crack tip governs the fractography of the materials. Furthermore, the material constant A_{NL} appears to be related to material toughness.

Although we only studied DN gels, we believe that the fractographic law discovered is universal and can be applied to other brittle fractures of soft materials. Therefore, it could be used to analyze soft material fractures in practical applications.

Author Contributions

R. K. and J. P. G. perceived the concept, designed the experiments, and interpreted the results. R. K. performed almost all the experiments and analyzed the data. Y. Z. performed pure shear tests. All authors participated in the discussion. R. K., T. N., and J. P. G. prepared the manuscript.

Conflicts of interest

There are no conflicts to declare.

Acknowledgements

J. P. G. thanks JSPS KAKENHI (Grant No. JP22H04968 and JP22K21342). The Institute for Chemical Reaction Design and Discovery (ICReDD) was established by the World Premier International Research Initiative (WPI) of MEXT, Japan. The authors thank the late Daniel R. King for his helpful comments.

References

1. O. Erol, A. Pantula, W. Liu, D. H. Gracias, Transformer Hydrogels: A Review. *Adv. Mater. Technol.* **4**, 1900043 (2019).
2. J. P. Gong, Friction and lubrication of hydrogels—its richness and complexity. *Soft Matter*. **2**, 544–552 (2006).
3. R. A. Green, S. Baek, L. A. Poole-Warren, P. J. Martens, Conducting polymer-hydrogels for medical electrode applications. *Sci. Technol. Adv. Mater.* **11**, 014107 (2010).
4. A. S. Hoffman, Hydrogels for biomedical applications. *Adv. Drug Deliv. Rev.* **64**, 18–23 (2012).
5. K. Y. Lee, D. J. Mooney, Hydrogels for Tissue Engineering. *Chem. Rev.* **101**, 1869–1880 (2001).
6. K. Yasuda, N. Kitamura, J. P. Gong, K. Arakaki, H. J. Kwon, S. Onodera, Y. M. Chen, T. Kurokawa, F. Kanaya, Y. Ohmiya, Y. Osada, A Novel Double-Network Hydrogel Induces Spontaneous Articular Cartilage Regeneration in vivo in a Large Osteochondral Defect. *Macromol. Biosci.* **9**, 307–316 (2009).
7. J. P. Gong, Y. Katsuyama, T. Kurokawa, Y. Osada, Double-network hydrogels with extremely high mechanical strength. *Adv. Mater.* **15**, 1155–1158 (2003).
8. J. P. Gong, Why are double network hydrogels so tough? *Soft Matter*. **6**, 2583–2590 (2010).
9. Y. Okumura, K. Ito, The Polyrotaxane Gel: A Topological Gel by Figure-of-Eight Cross-links. *Adv. Mater.* **13**, 485–487 (2001).
10. T. Sakai, T. Matsunaga, Y. Yamamoto, C. Ito, R. Yoshida, S. Suzuki, N. Sasaki, M. Shibayama, U. Chung, Design and Fabrication of a High-Strength Hydrogel with Ideally Homogeneous Network Structure from Tetrahedron-like Macromonomers. *Macromolecules*. **41**, 5379–5384 (2008).
11. C. Creton, M. Ciccotti, Fracture and adhesion of soft materials: a review. *Reports Prog. Phys.* **79**, 046601 (2016).
12. R. Long, C.-Y. Hui, J. P. Gong, E. Bouchbinder, The Fracture of Highly Deformable Soft Materials: A Tale of Two Length Scales. *Annu. Rev. Condens. Matter Phys.* **12**, 71–94 (2021).
13. R. Long, C.-Y. Hui, Fracture toughness of hydrogels: measurement and interpretation. *Soft Matter*. **12**, 8069–8086 (2016).
14. C. Yang, T. Yin, Z. Suo, Polyacrylamide hydrogels. I. Network imperfection. *J. Mech. Phys. Solids*. **131**, 43–55 (2019).
15. E. Bouchbinder, T. Goldman, J. Fineberg, The dynamics of rapid fracture: instabilities, nonlinearities and length scales. *Reports Prog. Phys.* **77**, 046501 (2014).
16. I. Kolvin, J. M. Kolinski, J. P. Gong, J. Fineberg, How Supertough Gels Break. *Phys. Rev. Lett.* **121**, 135501 (2018).
17. Y. Zhou, J. Hu, P. Zhao, W. Zhang, Z. Suo, T. Lu, Flaw-sensitivity of a tough hydrogel under monotonic and cyclic loads. *J. Mech. Phys. Solids*. **153**, 104483 (2021).
18. T. L. Anderson, *Fracture Mechanics, Third Edition Fundamentals and Applications* (Taylor&Francis Group, LLC., 2005).
19. G. D. Quinn, "Guidelines for Measuring Fracture Mirrors" *Ceramic Transactions*, **199**, 163–187 (2007).
20. E. B. SHAND, Breaking Stress of Glass Determined from Dimensions of Fracture Mirrors. *J. Am. Ceram. Soc.* **42**, 474–477 (1959).
21. J. J. Mecholsky, R. W. Rice, S. W. Freiman, Prediction of Fracture Energy and Flaw Size in Glasses from Measurements of Mirror Size. *J. Am. Ceram. Soc.* **57**, 440–443 (1974).
22. R. C. Bradt, The Fractography and Crack Patterns of Broken Glass. *J. Fail. Anal. Prev.* **11**, 79–96 (2011).
23. J. J. Mecholsky, S. W. Freimam, R. W. Rice, Fracture surface analysis of ceramics. *J. Mater. Sci.* **11**, 1310–1319 (1976).
24. R. C. Bradt, Applying fractography and fracture mechanics to the energy and mass of crack growth for glass in the mirror region. *J. Eur. Ceram. Soc.* **34**, 3255–3262 (2014).
25. S. Seiffert, Origin of nanostructural inhomogeneity in polymer-network gels. *Polym. Chem.* **8**, 4472–4487 (2017).
26. E. H. Yoffe, LXXV. The moving griffith crack. *London, Edinburgh, Dublin Philos. Mag. J. Sci.* **42**, 739–750 (1951).
27. Y. Zhang, K. Fukao, T. Matsuda, T. Nakajima, K. Tsunoda, T. Kurokawa, J. P. Gong, Unique crack propagation of double network hydrogels under high stretch. *Extrem. Mech. Lett.* **51**, 101588 (2022).
28. R. Kiyama, M. Yoshida, T. Nonoyama, T. Sedlačík, H. Jinnai, T. Kurokawa, T. Nakajima, J. P. Gong, Nanoscale TEM Imaging of Hydrogel Network Architecture. *Adv. Mater.* **35**, 2208902 (2023).